An Analysis of Fracture Network Intersections from DFN Models and Data: Density Distribution, Topology, and Stereology

Etienne Lavoine, Philippe Davy, Caroline Darcel, Diego Mas Ivars

An Analysis of Fracture Network Intersections from DFN Models and Data: Density Distribution, Topology, and Stereology

Conference Paper · June 2021

CITATIONS
0

READS
9

4 authors:

Etienne Lavoine
Itasca Consultants SAS
7 PUBLICATIONS **6** CITATIONS
SEE PROFILE

Philippe Davy
French National Centre for Scientific Research
302 PUBLICATIONS **12,417** CITATIONS
SEE PROFILE

Caroline Darcel
65 PUBLICATIONS **1,578** CITATIONS
SEE PROFILE

Diego Mas Ivars
Svensk Kärnbränslehantering AB
69 PUBLICATIONS **1,372** CITATIONS
SEE PROFILE

DFNE 21–2351

An analysis of fracture network intersections from DFN models and data: density distribution, topology, and stereology

Lavoine, E. and Darcel, C.
Itasca Consultants SAS, Lyon, France
Davy, P.
Univ Rennes, CNRS, Géosciences Rennes, UMR 6118, Rennes, France
Mas Ivars, D.
Swedish Nuclear Fuel and Waste Management Company, Solna, Sweden
KTH Royal Institute of Technology, Division of Soil and Rock Mechanics, Stockholm, Sweden

ABSTRACT: Intersections between the fractures of a network defines its connectivity and constitute a key component both for the hydrogeological and mechanical behavior of fractured rock masses. Existing analyses of 2D field trace maps provide a framework for analyzing 2D fracture intersection distributions. In this paper, we perform a complete analysis of 3D fracture intersections distribution of various DFN models and investigate how it can be related to the 2D distribution of intersecting virtual outcrops. The DFN models are either fully random (with no correlation between fractures) or defined from a genetic process (named UFM model). By comparing with natural 2D field trace maps, we show that, unlike the fully random DFN model which produces only X intersections, the UFM model is quantitatively consistent with the intersection distribution observed on field trace maps. The analysis framework developed here can be used as a relevant metric to select DFN models in terms of connectivity and give insights on the 3D topology of fracture networks.

1. INTRODUCTION

Fracture connectivity plays a major role on the hydrogeological and mechanical behavior of fractured rock mass (Davy et al., 2018; De Dreuzy et al., 2001). Most studies focus on describing connectivity from a density description using percolation parameter (Berkowitz, 1995; Bour and Davy, 1998). It is also possible to quantify network connectivity from a topological approach as fracture intersections statistics can be easily established in 2D from outcrop observations (Sanderson and Nixon, 2015). In this kind of approach, the fracture network is described as a graph of nodes (representing fracture intersections and terminations), linked by fracture segments (Fig. 1.a). Nodes can thus correspond to isolated fracture tips, or T and X intersections. Those statistics can serve as a proxy to characterize fracture networks (Fig. 1.b), and even estimate their connectivity and hydrological behavior (Saevik and Nixon, 2017).

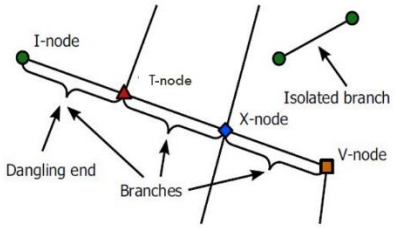

a)

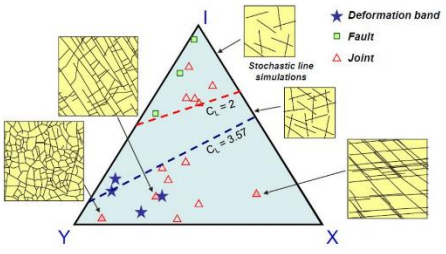

b)

Fig. 1. a) Typology of fracture nodes (tips and intersections) on 2D fracture networks. b) Ternary diagram of the proportion of node types for different 2D fracture networks. Modified from (Sanderson and Nixon, 2015)

In 3D, fracture intersections are line segments, terminations are fracture edges and it is not as obvious to

define a typology as the one presented in Fig. 1 (Sanderson et al., 2018). Moreover, we seriously lack direct observations on the geometry and nature of fracture intersections and the 3D vision of fracture intersections most of the time relies on 3D models of discrete fracture networks (DFN). Alghalandis et al. (2011) list all possible intersection situations (face-face, edge-face, edge-edge…) in a network made of polygonal fractures. Most of them are unlikely to occur in the widely used Poissonian models, where the fractures are generated independently of each other. The only way to obtain a wealth of fracture intersection types is to introduce correlations between fractures as it is in genetic DFN models, where fractures grow and stop according to their surrounding fractures. The UFM model of Davy et al. (2013), based on three simplified mechanical rules (nucleation, propagation, and arrest), introduces three types of fracture intersections: X, T-side, and T-plane intersections (Fig. 2).

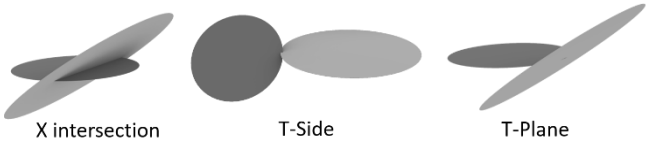

Fig. 2. Typology of fracture intersections in 3D, as defined in the UFM model

In this paper, we perform a complete analysis of the intersections between fractures, as they arise from entire fractures in 3D volumes, and as they can be observed from fracture traces seen on 2D sampling planes. We also aim to evaluate if the nature and distribution of intersections can be used as a relevant metric for selecting DFN models. Both field data (fracture trace maps) and DFN models are analyzed in the process. The DFN models are based on disc-shaped assumption for individual fractures. Hence, intersections in 3D can be viewed as segments whereas they are reduced to intersection points between fracture traces in 2D.

First, we show analytically and numerically how the 3D population of fracture intersections are related to the general DFN parameters such as fracture density and size distribution. Secondly, we perform the stereological analysis – 3D/2D- of the fracture intersections. We show that the number of fracture intersections observed in 2D is directly related to the total 3D intersection size. Finally, we show that, unlike the fully random DFN model which produces only X intersections, the UFM model is quantitatively consistent with the intersection distribution into T and X types otherwise observed on natural trace maps.

2. 3D DFN INTERSECTIONS STATISTICS

Because of the 2D nature of fracture data (outcrops), we do not have access directly to 3D intersections statistics from real fracture networks. Nevertheless, we can compute these statistics on 3D DFN models (stochastic and genetic) and use it as a reference. Intersection statistics can be established by computing the probability that fracture planes intersect in a given volume, considering their orientation and extension. To our knowledge, it only exists few studies about fracture intersections statistics in 3D. Barker (2018) provides a collection of formulae for the intersection of fracture planes with lines (boreholes or scanlines), outcrop planes, and with other fracture planes, considering any convex shape. It is then possible to derive statistics of intersections size for a given network of planar fractures. Alghalandis et al. (2011) show that an exponential distribution of fracture size leads to an exponential intersection size distribution resulting in more small intersections than large ones. We show here that 3D fracture intersections typology and statistics are a consequence of our models (Poissonian and UFM) that can be estimated from input parameters.

2.1 Poissonian DFN

A Poissonian DFN assumes that fractures are randomly positioned in the target generation volume with a prescribed size and orientation probability distribution and a total fracture intensity p_{32} (i.e., the total fracture surface divided by the generation volume). We define 6 different Poissonian DFN models of same fracture density $p_{32} = 0.5\ m^{-1}$, with fractured contained in cubic systems of size $L = 100\ m$, all following uniform orientation distribution, but different sizes distributions:

- Constant fracture size $l_f = 10\ m$
- Power-law size distribution of exponent $a = [3.0,3.2,3.4,3.8,4.0,4.4]$ ranging from $l_{min} = 1\ m$ to $l_{max} = 50\ m$

For each model we perform 10 realizations to compute network statistics. Fig. 3 shows the intersection size distributions for each realization of each model.

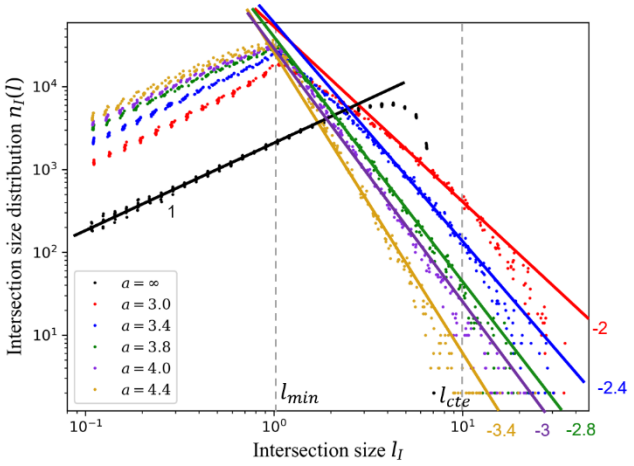

Fig. 3. Intersection size distribution for 3D Poissonian DFNs following various size distribution. Lines are drawn to fit results.

For all models, the intersection size distribution follows a linear relationship for intersections sizes smaller than the minimum fracture size. For DFNs following a power-law fracture size distribution $n(l_f) \sim l_f^{-a}$, the intersection size distribution $n_I(l_I)$ also follows a power-law relationship of equation:

$$n_I(l_I) \sim l_f^{-a+1} \quad (1)$$

In addition, we demonstrate that the total volumetric intersection length $p_{31,I}$ is only related to the DFN density p_{32} with the following relationship (see Appendix):

$$p_{31,I} = \int n_I(l_I) l_I dl_I = \frac{k_\theta . k_{l_I}}{2\beta_f} . (p_{32})^2 \quad (2)$$

with k_θ an orientation factor, k_{l_I} the ratio between the intersection size and the size of the smallest intersecting fracture, and β_f a fracture shape factor ($\pi/4$ for disc-shaped fractures). If the fracture orientation distribution is uniform, $k_\theta = 2/\pi$.

Thus, the total fracture intersection length $p_{31,I}$ is independent of the fracture size distribution exponent (Fig. 4).

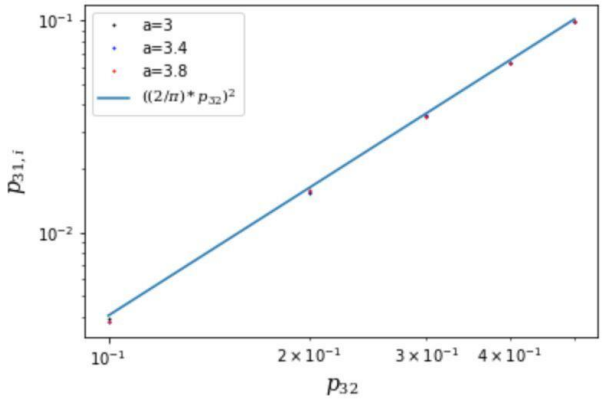

Fig. 4. Evolution of total intersection length per unit volume $p_{31,I}$ with fracture density p_{32}

2.2 UFM DFN

The UFM model is a genetic DFN model based on three basic processes: nucleation, fracture growth, and arrest. A detailed description of the model is given in (Davy et al., 2013). One main characteristic of the UFM model is that generated DFNs contain both T and X intersections, while Poissonian DFNs have only X intersections. According to the arrest rule (a fracture cannot cross a larger one, but the reverse is possible), X intersections occur when large fractures propagate through smaller ones while T intersections occur when a small fracture is blocked by larger ones.

We perform here the same kind of analysis as above on UFM DFNs. Growth parameters are chosen so that the fracture size distribution is a double power-law, composed of a dilute regime – i.e., small fractures that are not abutting another fracture on average – of exponent $a_d = 3$, and a dense regime – large fractures that are almost all abutting another one – of exponent $a_D = 4$, with minimum fracture size $l_n = 1\ m$, and a transition length $l_c = 4\ m$. Finally, T intersections are set to be 20% of the abutting fracture size. To study UFM models properly, we compare the obtained intersection size distribution with the one of an equivalent Poissonian model (obtained by randomizing fracture positions, thus breaking fracture correlations). For both models we generate 10 realizations for statistical analysis. We summarize fractures and intersections statistics in Table 1.

Table 1. Fracture and intersections statistics of the UFM and equivalent Poissonian models

	UFM	Poissonian
Fracture number	103 000	103 000
Fracture density	0.9	0.9
Intersection number	145 000	181 000
T-Plane	*35%*	
T-Side	*11%*	
X	*54%*	*100%*

For the selected parameters set, the UFM model shows 55% of X intersections and 45% of T intersections. We also notice that it has less intersections in total than its equivalent Poissonian model. Fig. 5 shows the volumetric intersection size distribution. The UFM has more small intersections (which corresponds mainly to T intersections), and less large intersections.

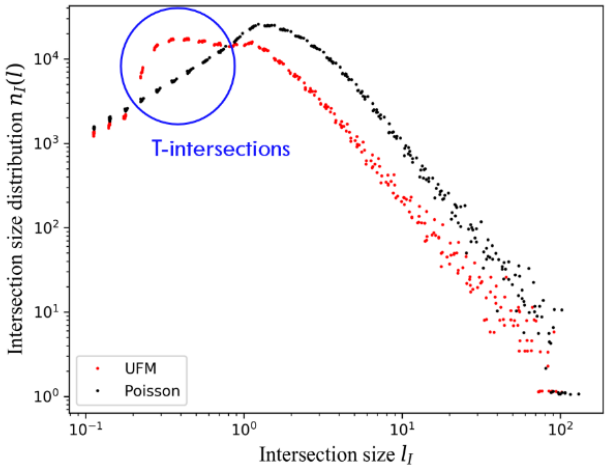

Fig. 5. Intersection size distribution for the UFM and equivalent Poisson DFN

3. STEREOLOGICAL ANALYSIS OF FRACTURE INTERSECTIONS

This section aims to relate both 3D and 2D intersections statistics by performing a stereological analysis. Stereological rules development relies on the definition of

the intersection probability between 3D DFN and 2D observation planes.

3.1 Poissonian DFN

We first perform a stereological analysis on Poissonian DFN models defined in the previous section. In 3D, the fracture network is described as a set of discs, and intersections are segments. Fracture traces with an observation plane are thus segments, and intersections are points (Fig. 6).

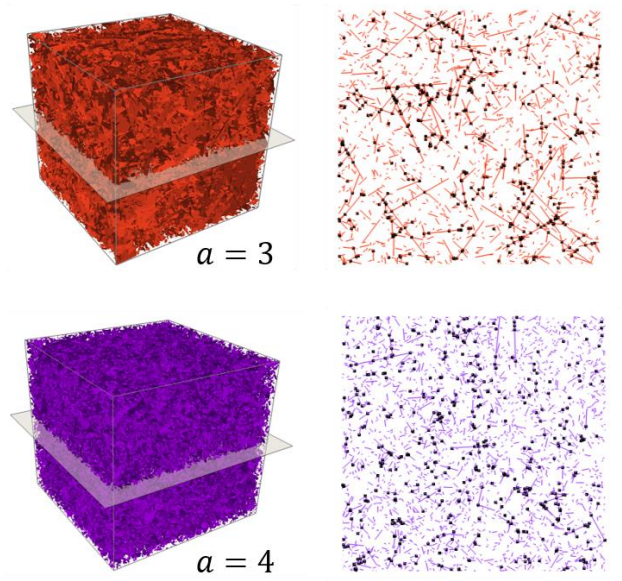

Fig. 6. Comparison between 3D Poissonian DFN and traces with an observation plane for two different exponent of power-law size distribution.

To analyze intersections statistics both in 3D and 2D for all DFNs, we compute the following indicators:

- $p_{20,I}$: number of fracture intersections per unit outcrop area (2D)
- $p_{30,I}$: number of fracture intersections per unit volume (3D)
- $p_{31,I}$: cumulated intersection length per unit volume (3D)

Fig.7 shows that $p_{20,I}$ and $p_{31,I}$ are independent of the fracture size distribution parameters. The ratio $p_{20,I}/p_{31,I}$ (0.5 here) should only depend on the fracture orientation distribution. Since we demonstrated in the previous Section that $p_{31,I}$ is only dependent on p_{32}, we conclude that one should be able to estimate the DFN p_{32} by counting the number of fracture intersections per unit of outcrop area.

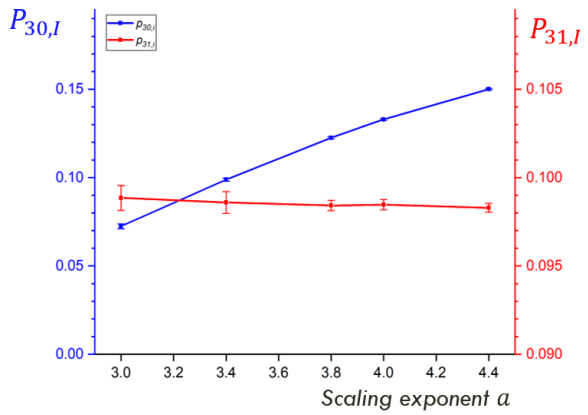

a)

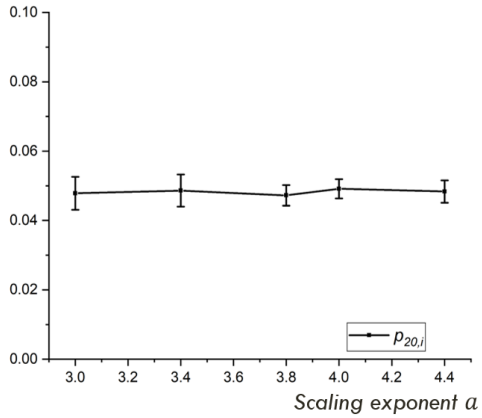

b)

Fig.7. Evolution of a) $p_{30,I}$ and $p_{31,I}$ and b) $p_{20,I}$ with fracture size power-law exponent a

3.2 UFM DFN

We proceed to the same kind of analysis on the UFM DFNs generated in the previous Section. Fig. 8 shows virtual outcrops of UFM and equivalent Poissonian DFN, with identified intersections. The two patterns look very different. Fracture intersections are much more homogeneously distributed in space for the UFM model in comparison to the Poissonian model. This is due to the difference in fracture density variability between the two models (Lavoine, 2020; Lavoine et al., 2019).

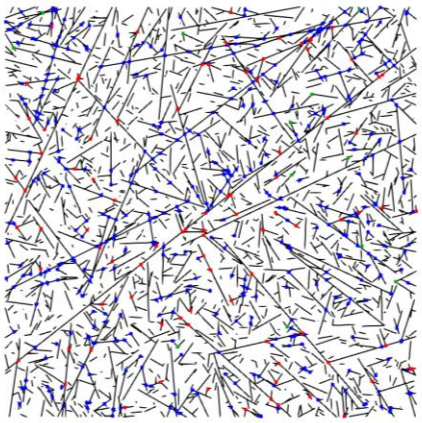

a)

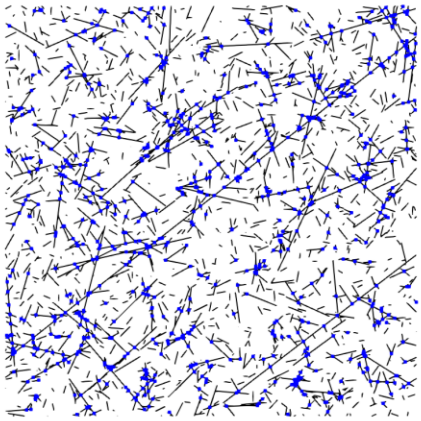

b)

Fig. 8. Virtual outcrops and identified intersection (X in blue, T-plane in red, T-side in green) for a a) UFM and an b) equivalent Poissonian model

Table 2 shows intersections indicators values both for the UFM and their corresponding equivalent Poissonian DFNs. The percentage of T intersections observed on the virtual outcrop is only 21% of all intersections (against 55% in 3D). This percentage may strongly depend on the size of T intersections, which is an input of the UFM model. Indeed, if this size is set to 0, there will be no T intersections in 2D while they exist in 3D as points. For both models, the ratio $p_{20,I}/p_{31,I}$~0.5. For the UFM model, this ratio is the same if looking at T or X intersections exclusively. This means that, knowing the fracture orientation distribution (and thus fracture intersection orientation distribution), one may be able to assess the total T and X intersection total length per unit volume in the volume domain.

Table 2. Fracture intersections indicators obtained for the UFM (X and T) and the equivalent Poissonian models

Model	$p_{31,I}$	$p_{30,I}$	$p_{20,I}$
UFM	0.1080	0.1225	0.0510
T intersections	0.0231	0.0429	0.0108
X intersecions	0.0849	0.0796	0.0402
Poissonian	0.1791	0.1221	0.0868

4. THE FRACTURE INTERSECTION TYPOLOGY DIAGRAM IN MODELS AND OUTCROPS

4.1 Analysis of natural trace maps

In this Section, we perform 2D analysis of fracture traces from real outcrops from the Laxemar site in Sweden in the same spirit as the ternary diagram shown in Fig. 1. For each outcrop, traces are stored as individual polylines, associated to an attribute table for properties (e.g. apparent dip and strike). Fig. 9.a shows an example of trace map from outcrop ASM000206. The system size is about 25 meters and the mapping resolution (which fixes the minimum fracture trace length) is 0.5 meter. Fractures are colored by their number of T intersections (0, 1 or 2). To do so, we develop a procedure to compute the I, X and T nodes from fracture traces polylines. In this procedure, we identify T configurations even if the T branching is not "perfect" (due to mapping and recording limits). For each fracture, we compute potential T-intersection for both tips. To do so, we compute the smallest distance d between each fracture tip and the rest of the DFN ($d < 0$ if intersection exists, otherwise $d > 0$). Then we determine threshold values ϵ and d_{max}, to consider the tip to be a T intersection or not. To do so, we apply the algorithm to a randomized version of the dataset. The frequency distribution of distance d for the real dataset and its radomized version are then used to define the threshold values as randomized DFNs are not supposed to show T intersections (Fig. 9.b). We apply this algorithm to several outcrops and report them in a fracture node ternary diagram (Fig. 9.c).

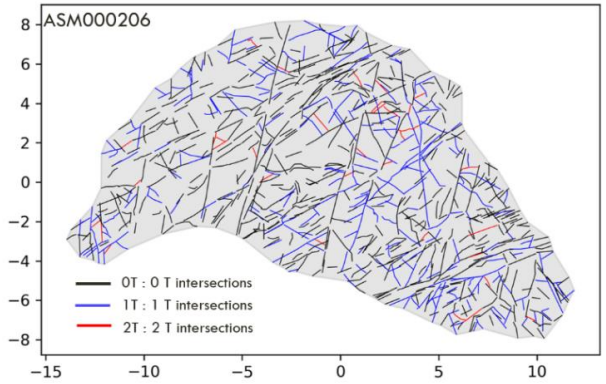

a)

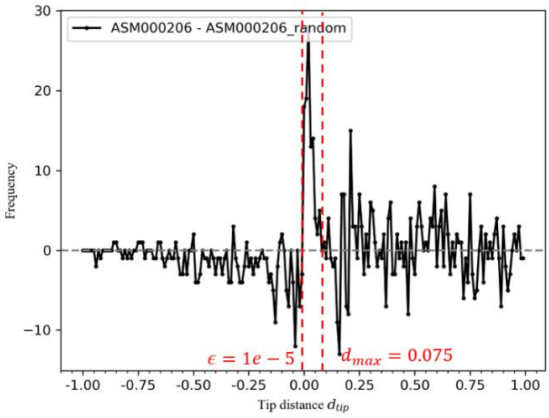

b)

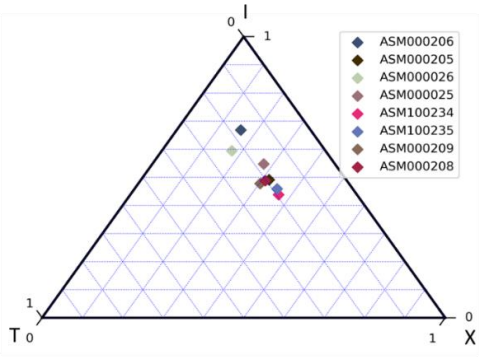

c)

Fig. 9. a) Example of outcrop (ASM000206) with fracture colored by number of T terminations. b) Difference between frequency distribution of distance d for the real dataset and its radomized version. c) Ternary diagram of the proportion of node types for the analysed Laxemar outcrops

4.2 Comparison with genetic models

To check the consistency of the UFM model in reproducing the intersections distribution of natural outcrops, we generate a UFM DFN, whose generation parameters are chosen so that orientation and size distribution of fractures cutting a virtual outcrop reproduce statistics of Laxemar site. To avoid the effect of fixing T intersection size in the UFM model as identified in the Section 3.b, we set the T intersection size to be 0 and apply the T intersection detection algorithm described above. Fig. 10 shows an example of a UFM DFN virtual outcrop.

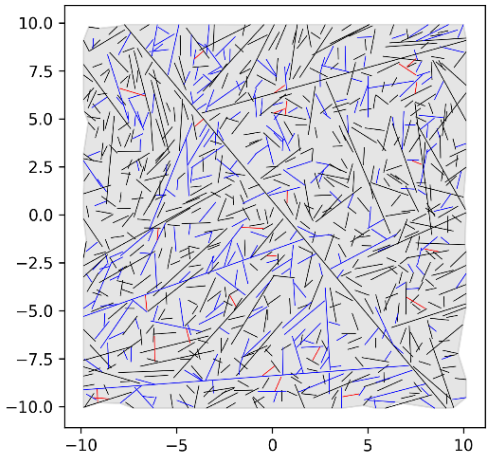

a)

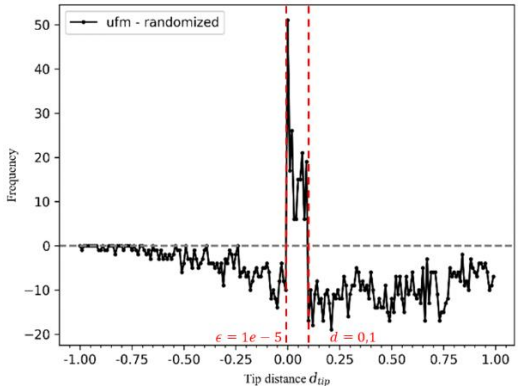

b)

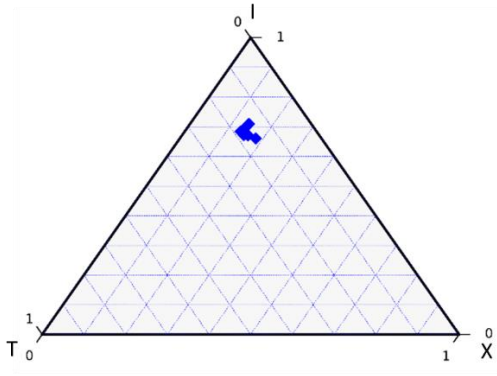

c)

Fig. 10. a) Example of a UFM virtual outcrop with fractures colored by number of T terminations. b) Difference between frequency distribution of distance d for the UFM dataset and its radomized version. c) Ternary diagram of the proportion of node types for the generated UFM virtual outcrops

The proportion of isolated tips, X and T intersections observed on virtual outcrops is consistent with the ones of natural trace maps from Laxemar. This cannot be the unique criteria for checking the validity of the UFM model to represent natural fracture network but, at least, this is a test passed by the model.

5. CONCLUSION

In this paper, we performed a full 3D analysis of fracture intersections population from various models (Poisson statistics and genetic). We have shown that, whatever the model, intersections density is directly related to the fracture density. Moreover, our stereological analysis of the problem has shown that the intersection density $p_{20,I}$ observed from 2D observation planes only depends on the 3D intersection density $p_{31,I}$, which is also a function of fracture density. Finally, we propose a classification of fracture tips in T, X and I from an intersection detection algorithm, which was applied both on natural fracture trace maps and virtual outcrops from DFN models. We show that the 2D intersection population obtained with the UFM model is consistent with natural observations from the intersection typology point of view.

All these elements suggest that:

- it may be possible to have an insight of the 3D intersection population of natural fracture networks by measuring the T and X intersections density ($p_{20,I,T}$ and $p_{20,I,X}$) from available outcrops, in addition to the classical fracture size and orientation distributions
- it may be possible to test whether models are consistent with data from the intersection point of view.

ACKNOWLEDGMENTS

This work is funded by Svensk Kärnbränslehantering AB, the Swedish Nuclear Fuel and Waste Management Company.

APPENDIX

We show here that, for 3D Poissonian DFNs, the total volumetric intersection length $p_{31,I}$ is only related to the fracture density p_{32} with the following relationship (see Section 1.a):

$$p_{31,I} = \frac{k_\theta k_{l_I}}{2\beta_f} p_{32}^2 \tag{3}$$

We consider that the fracture size and orientation distributions are independent so that:

$$n(l,\theta) = n(l)n(\theta) \tag{4}$$

The probability for a fracture of size l', following an orientation distribution $n(\theta)$, to intersect a fracture of size l, contained in a volume V, is:

$$p(l,l') = \frac{1}{V}\beta_f l^2 \left(l' \frac{\int_0^\pi n(\theta) sin(\theta) d\theta)}{\pi} \right) = \frac{k_\theta \beta_f l^2 l'}{V} \tag{5}$$

with β_f a shape factor so that the fracture surface is $\beta_f l^2$. The number of intersections between an ensemble of fractures of size $\in [l', l'+dl']$ with a fracture of size l is:

$$N_I(l,l') = p(l,l')n(l')dl'V = k_\theta \beta_f l^2 n(l') l' dl' \tag{6}$$

Let l_I be the intersection size, the cumulated intersection length of fractures intersecting a larger fracture of size l is:

$$L_I(l,l') = \int_{l'<l} N_I(l,l') l_i \, dl' \tag{7}$$

$$L_I(l,l') = k_\theta \beta_f l^2 \int_{l'<l} n(l') l' l_I \, dl' \tag{8}$$

The total intersection size per unit volume $p_{31,I}$ is obtained by integrating over the whole fracture size distribution:

$$p_{31,I} = \int_l \; n(l) L_I(l,l') dl \tag{9}$$

Considering the intersections size to be proportional to the smallest intersecting fracture $l_I = k_{l_I} \, l'$, we finally obtain:

$$p_{31,I} = \beta_f k_\theta k_{l_I} \int_l \; n(l) l^2 \left(\int_{l'<l} n(l') l'^2 \, dl' \right) dl \tag{10}$$

$$p_{31,I} = \frac{k_\theta k_{l_I}}{2\beta_f} p_{32}^2 \tag{11}$$

with the fracture density $p_{32} = \int_l \; n(l) \beta_f l^2 dl$.

REFERENCES

1. Alghalandis, Y. F., C. Xu, and P. A. Dowd, A general framework for fracture intersection analysis: algorithms and practical applications, *in* Proceedings Proc, Australian Geothermal Energy Conference, Melbourne2011, p. 15-20.
2. Barker, J. A., 2018, Intersection statistics and percolation criteria for fractures of mixed shapes and sizes: Computers & Geosciences, v. 112, p. 47-53.
3. Berkowitz, B., 1995, Analysis of fracture network connectivity using percolation theory: Mathematical Geology, v. 27, no. 4, p. 467-483.
4. Bour, O., and P. Davy, 1998, On the connectivity of three-dimensional fault networks: Water Resources Research, v. 34, no. 10, p. 2611-2622.
5. Davy, P., C. Darcel, R. Le Goc, and D. Mas Ivars, 2018, Elastic Properties of Fractured Rock Masses With Frictional Properties and Power Law Fracture Size Distributions: Journal of Geophysical Research: Solid Earth.
6. Davy, P., R. Le Goc, and C. Darcel, 2013, A model of fracture nucleation, growth and arrest, and consequences for fracture density and scaling: Journal of Geophysical Research: Solid Earth, v. 118, no. 4, p. 1393-1407.
7. De Dreuzy, J.-R., P. Davy, and O. Bour, 2001, Hydraulic properties of two-dimensional random fracture networks following a power law length distribution: 1. Effective connectivity: Water Resources Research, v. 37, no. 8, p. 2065-2078.
8. Lavoine, E., 2020, Modélisation cinématique et mécanique des réseaux de fractures à l'échelle du massif rocheux: Rennes 1.
9. Lavoine, E., P. Davy, C. Darcel, and R. Le Goc, 2019, On the Density Variability of Poissonian Discrete Fracture

Networks, with application to power-law fracture size distributions: Advances in Geosciences, v. 49, p. 77-83.
10. Saevik, P. N., and C. W. Nixon, 2017, Inclusion of Topological Measurements into Analytic Estimates of Effective Permeability in Fractured Media: Water Resources Research, v. 53, no. 11, p. 9424-9443.
11. Sanderson, D. J., and C. W. Nixon, 2015, The use of topology in fracture network characterization: Journal of Structural Geology, v. 72, p. 55-66.
12. Sanderson, D. J., D. C. Peacock, C. W. Nixon, and A. Rotevatn, 2018, Graph theory and the analysis of fracture networks: Journal of Structural Geology.